JOURNAL OF THE AMERICAN COLLEGE OF CARDIOLOGY
© 2017 BY THE AMERICAN COLLEGE OF CARDIOLOGY FOUNDATION
PUBLISHED BY ELSEVIER

VOL. 70, NO. 4, 2017
ISSN 0735-1097/$36.00
http://dx.doi.org/10.1016/j.jacc.2017.05.053

Magnetic Resonance in Transthyretin Cardiac Amyloidosis

Ana Martinez-Naharro, MD,[a,b] Thomas A. Treibel, MBBS,[c,d] Amna Abdel-Gadir, MBBS,[c,d] Heerajnarain Bulluck, MBBS,[e] Giulia Zumbo, MD,[a] Daniel S. Knight, MBBS,[a] Tushar Kotecha, MBChB,[a,c] Rohin Francis, MBBS,[a,e] David F. Hutt, BAPSc,[a] Tamer Rezk, MBBS,[a] Stefania Rosmini, MD,[d] Candida C. Quarta, MD, PhD,[a] Carol J. Whelan, MD,[a] Peter Kellman, PhD,[f] Julian D. Gillmore, MD, PhD,[a,b] James C. Moon, MD,[c,d] Philip N. Hawkins, PhD,[a,b] Marianna Fontana, PhD[a,b,c]

ABSTRACT

BACKGROUND Cardiac transthyretin amyloidosis (ATTR) is an increasingly recognized cause of heart failure. Cardiac magnetic resonance (CMR), with late gadolinium enhancement (LGE) and T1 mapping, is emerging as a reference standard for diagnosis and characterization of cardiac amyloidosis.

OBJECTIVES The authors used CMR with extracellular volume fraction (ECV) measurement to characterize cardiac involvement in relation to outcome in ATTR.

METHODS Subjects comprised 263 patients with cardiac ATTR corroborated by grade 2 to 3 ^{99m}Tc-DPD (^{99m}Tc-3,3-diphosphono-1,2-propanodicarboxylic acid) cardiac uptake, 17 with suspected cardiac ATTR (grade 1 ^{99m}Tc-DPD), and 12 asymptomatic individuals with amyloidogenic transthyretin (TTR) mutations. Fifty patients with cardiac light-chain (AL) amyloidosis acted as disease comparators.

RESULTS Unlike cardiac AL amyloidosis, asymmetrical septal left ventricular hypertrophy (LVH) was present in 79% of patients with ATTR (70% sigmoid septum and 30% reverse septal contour), whereas symmetrical LVH was present in 18%, and 3% had no LVH. In patients with cardiac amyloidosis, the pattern of LGE was always typical for amyloidosis (29% subendocardial, 71% transmural), including right ventricular LGE (96%). During follow-up (19 $\pm$ 14 months), 65 patients died. ECV independently correlated with mortality and remained independent after adjustment for age, N-terminal pro-B-type natriuretic peptide, ejection fraction, E/E′, and left ventricular mass (hazard ratio: 1.164; 95% confidence interval: 1.066 to 1.271; $p < 0.01$).

CONCLUSIONS Asymmetrical hypertrophy, traditionally associated with hypertrophic cardiomyopathy, was the commonest pattern of ventricular remodeling in ATTR. LGE imaging was typical in all patients with cardiac ATTR. ECV correlated with amyloid burden and was an independent prognostic factor for survival in this cohort of patients. (J Am Coll Cardiol 2017;70:466–77) © 2017 by the American College of Cardiology Foundation.

Cardiac transthyretin amyloidosis (ATTR) is a progressive and fatal form of amyloidosis caused by extracellular deposition of amyloid fibrils from liver-derived transthyretin (TTR) (1). ATTR can be hereditary, in which genetic variants of TTR are implicated and are associated with the overlapping syndromes of familial amyloid cardiomyopathy and familial amyloid polyneuropathy, or it can be sporadic, associated with deposition of wild-type transthyretin as amyloid. The latter predominantly

Listen to this manuscript's audio summary by *JACC* Editor-in-Chief Dr. Valentin Fuster.

From the [a]National Amyloidosis Centre, University College London, Royal Free Hospital, London, United Kingdom; [b]Division of Medicine, University College London, London, United Kingdom; [c]Institute of Cardiovascular Science, University College London, London, United Kingdom; [d]Barts Heart Centre, West Smithfield, London, United Kingdom; [e]The Hatter Cardiovascular Institute, Institute of Cardiovascular Science, University College London, United Kingdom; and the [f]National Heart, Lung, and Blood Institute, National Institutes of Health, Bethesda, Maryland. Dr. Gillmore is an advisory board member for GlaxoSmithKline. Prof. Moon has received an unrestricted research grant from GlaxoSmithKline; and has been paid a consultancy fee for trial design. All other authors have reported that they have no relationships relevant to the contents of this paper to disclose.

Manuscript received February 21, 2017; revised manuscript received May 21, 2017, accepted May 24, 2017.

involves the hearts of older people, and the disorder is also known as senile systemic amyloidosis. At autopsy, cardiac ATTR amyloid deposition can be remarkably common, present in 8% to 16% of individuals older than 80 years (2). Conversely, cardiac ATTR is rarely diagnosed during life, but greater awareness and better imaging methods have increased its recognition lately among elderly patients with left ventricular hypertrophy (LVH) and in specific at-risk ethnic populations (3).

SEE PAGE 478

Diagnosing cardiac ATTR amyloidosis is challenging. A suggestive constellation of electrocardiography, echocardiography, and biomarker findings are present in advanced disease, but interpretation can be confounded by common comorbidities such as hypertensive heart disease, diabetes mellitus, diastolic dysfunction, and renal disease (4–6). Bone tracer scintigraphy, using ^{99m}Tc-DPD (^{99m}Tc-3,3-diphosphono-1,2-propanodicarboxylic acid), ^{99m}Tc-PYP (^{99m}Tc-pyrophosphate), and ^{99m}Tc-HMDP (^{99m}Tc-hydroxymethylene diphosphonate), has recently emerged as a sensitive tool for the identification of cardiac ATTR (7–9); however, this nuclear medicine method is typically only performed to confirm ATTR when a clinical suspicion exists, because it does not provide information on any of the other differentials of LVH, cardiac morphology, or function and is semiquantitative only (10), a limitation given the development of therapies able to stop or remove cardiac amyloid deposits (9,11).

In the past decade, cardiac magnetic resonance (CMR) has emerged as a robust imaging technique that provides detailed information about the presence, location, and distribution of hypertrophy, as well as visualization of cardiac amyloid infiltration with late gadolinium enhancement (LGE) imaging and measurement of cardiac amyloid burden with T1 mapping and extracellular volume (ECV) (12–18). One retrospective study in patients with cardiac amyloidosis (n = 51) suggested that a high proportion of patients have morphological phenotypes that differ from the classic description of concentric symmetric hypertrophy (19), but the amyloidosis type was not specified. No study has assessed the morphology in a large cohort of patients with ATTR. ECV has been shown to be an important marker of prognosis in patients with AL amyloidosis, but its prognostic significance has never been assessed in patients with ATTR.

The aim of this study was to examine the CMR morphological phenotypes and tissue characterization findings in ATTR, correlate these with clinical outcomes, and compare these findings with AL amyloidosis.

METHODS

Ethical approval was granted by the University College London/University College London Hospitals Joint Committees on the Ethics of Human Research Committee, and all participants provided written informed consent.

A total of 342 subjects were prospectively recruited between 2011 and 2015. The study population underwent comprehensive clinical evaluation and follow-up at the National Amyloidosis Centre, London, United Kingdom, and comprised the 3 groups described below. Patients were systematically followed up until October 4, 2016, the date of censoring.

Cardiac ATTR was defined as the combination of symptoms with an echocardiogram consistent with or suggestive of cardiac amyloidosis, grade 2 or 3 cardiac uptake on ^{99m}Tc-DPD scintigraphy in the absence of monoclonal gammopathy, or in the presence of monoclonal gammopathy, a cardiac biopsy positive for TTR (9). Suspected cardiac ATTR was defined by grade 1 cardiac uptake on ^{99m}Tc-DPD scintigraphy in the absence of monoclonal gammopathy. All subjects underwent sequencing of exons 2, 3, and 4 of the *TTR* gene.

We recruited 263 consecutive patients (227 men; age 74 ± 9 years) with cardiac ATTR and 17 with suspected cardiac ATTR. *TTR* gene mutation carriers were defined as individuals with no evidence of clinical disease (no cardiac uptake on ^{99m}Tc-DPD scintigraphy and normal echocardiography, CMR, N-terminal pro-B-type natriuretic peptide [NT-proBNP], and troponin T). Twelve *TTR* gene mutations carriers were recruited (4 men; age 47 ± 11 years). Cardiac AL amyloidosis was determined on the basis of international consensus criteria (20), and 50 consecutive patients with cardiac AL amyloidosis (37 men; age 63 ± 10 years) were recruited as a comparator group. Subjects with contraindications to CMR included those with a glomerular filtration rate <30 ml/min.

CMR PROTOCOL. All participants underwent standard CMR on a 1.5-T clinical scanner. A standard volume and LGE study was performed. The gadolinium-based contrast agent used was 0.1 mmol/kg gadoterate meglumine. LGE imaging was acquired with magnitude reconstruction in all patients and with phase-

ABBREVIATIONS AND ACRONYMS

^{99m}Tc-DPD = ^{99m}Tc-3,3-diphosphono-1,2-propanodicarboxylic acid

AL = light-chain amyloidosis

ATTR = transthyretin amyloidosis

ATTRm = hereditary transthyretin amyloidosis

CI = confidence interval

CMR = cardiac magnetic resonance

CT = computed tomography

ECV = extracellular volume fraction

HR = hazard ratio

LGE = late gadolinium enhancement

LV = left ventricular

LVH = left ventricular hypertrophy

MOLLI = modified Look-Locker inversion recovery

NT-proBNP = N-terminal pro-B-type natriuretic peptide

RV = right ventricle

SPECT = single-photon emission computed tomography

TTR = transthyretin

sensitive inversion recovery reconstruction (PSIR) in 82% of patients. For native T1 and post-contrast mapping, basal and midventricular short-axis and 4-chamber long-axis images were acquired by the modified Look-Locker inversion recovery (MOLLI) or shortened MOLLI sequence after regional shimming, as described previously (21). After the bolus of gadoterate meglumine and standard LGE imaging (standard fast low-angle shot inversion recovery or balanced steady-state free-precession sequence with magnitude reconstruction and PSIR reconstruction), the T1 measurement was repeated with the MOLLI or shortened MOLLI sequence (22). In 17 patients with ATTR, a post-contrast T1 map acquisition was not performed; 5 patients requested the scan be terminated early, and 12 had claustrophobia.

CMR IMAGE ANALYSIS. All CMR images and maps were analyzed offline. The presence of LVH was defined as increased left ventricular (LV) mass based on age- and sex-indexed reference values. Asymmetrical septal hypertrophy was defined as a ratio between the septal and posterior wall >1.5 (19). Asymmetrical septal hypertrophy comprised, in turn, 2 different patterns: 1) sigmoid septum, with the septum being concave to the LV cavity and a prominent basal septal bulge; and 2) reverse septal contour, with an abnormal convexity of the septum toward the LV cavity (23,24). A ratio between the septal and posterior wall ≤1.5 with increased mass was considered symmetrical concentric LVH.

T1 measurement was performed by drawing a region of interest in the basal to mid septum of the appropriate 4-chamber map. For ECV measurement, a single region of interest was drawn in each of the 4 required areas: myocardial T1 estimates (basal to mid septum in 4-chamber map) and blood T1 estimates (LV cavity blood pool in 4-chamber map, avoiding the papillary muscles) before and after contrast administration. Hematocrit was measured in all subjects immediately before each CMR study. ECV was calculated as: myocardial ECV = (1 − hematocrit) × ($\Delta R1_{myocardium}$ / $\Delta R1_{blood}$), where R1 = 1 / T1.

Before our adoption of PSIR for all amyloidosis patients, because myocardial nulling can be difficult in the presence of amyloid, any confusion with magnitude reconstruction images was resolved by selecting the images that most closely matched the post-contrast T1 maps, with "bright" LGE expected to correlate with areas of the lowest post-contrast T1 (i.e., the highest gadolinium concentration, the highest interstitial expansion).

The LGE pattern was classified into 3 groups according to the degree of transmurality: group 1, no LGE; group 2, subendocardial LGE (when there was global subendocardial but no transmural LGE); and group 3, transmural LGE (when the LGE extended transmurally). Thus, a patient with basal transmural LGE but apical subendocardial LGE would be classified as having transmural LGE (25).

^{99M}Tc-DPD SCINTIGRAPHY. Subjects were scanned with hybrid single-photon emission computed tomography (SPECT) computed tomography (CT) gamma cameras after administration of 700 MBq of intravenously injected ^{99m}Tc-DPD. Whole-body planar images were acquired after 3 h, followed by SPECT of the heart coupled with a low-dose, non-contrast CT scan as described previously (26). Gated and nongated cardiac SPECT reconstruction and SPECT-CT image fusion were performed on the Xeleris workstation (GE Healthcare, Wauwatosa, Wisconsin). Cardiac retention of ^{99m}Tc-DPD was scored visually according to the grading devised by Perugini et al. (27) using the following grading system: grade 0, absent cardiac uptake; grade 1, mild cardiac uptake less than bone; grade 2, moderate cardiac uptake equal or greater than bone; and grade 3, intense cardiac uptake associated with substantial reduction or loss of bone signal.

STATISTICAL ANALYSIS. Statistical analysis was performed with IBM SPSS Statistics version 22 (IBM, Armonk, New York). All continuous variables were normally distributed (Shapiro-Wilk test), other than NT-proBNP, which was natural log transformed for bivariate testing. These are presented as mean ± SD, with non-natural log-transformed NT-proBNP presented as median and interquartile range. Comparisons between groups were performed by 1-way analysis of variance with post hoc Bonferroni correction. The chi-square test or Fisher exact test was used to compare categorical data as appropriate. Correlations between parameters were assessed with Pearson (r) or Spearman's rho. Statistical significance was defined as $p < 0.05$.

Survival was evaluated by Cox proportional hazards regression analysis, which provided estimated hazard ratios (HRs) with 95% confidence intervals (CIs) and Kaplan-Meier curves. HRs were estimated for predefined increments or decrements in the variables based on clinically relevant changes or published normative data guidelines. All variables were selected a priori for clinical relevance: ECV as a marker of amyloid infiltration; ejection fraction for systolic function; E/E′ for diastolic function; LV mass for structural changes; and NT-proBNP as a blood biomarker. A multivariable model was used to investigate factors associated with overall survival.

TABLE 1 Patient Characteristics

	All ATTR Subjects (N = 292)	Tc-DPD Grade 0 (n = 12)	Tc-DPD Grade 1 (n = 17)	Tc-DPD Grade 2 (n = 204)	Tc-DPD Grade 3 (n = 59)	AL (n = 50)
Age, yrs	72 ± 11	47 ± 11	70 ± 14	75 ± 8	72 ± 11*	63 ± 10†
Comorbidities						
Diabetes mellitus	7	0	0	8	7	0†
Hypertension	17	0	24	18	14	10†
Ischemic heart disease	10	0	18	13	2	10
Biomarkers						
NT-proBNP, ng/l	1,886 (576-1,217)	21 (10-31)	247 (47-288)	2,001 (690-2,168)	2,342 (741-3,683)*	1,886 (575-2,168)
Echocardiographic parameters						
IVS, cm	1.61 ± 0.29	0.95 ± 0.12	1.12 ± 0.28	1.65 ± 0.22	1.72 ± 0.24*	1.49 ± 0.18†
LPW, cm	1.31 ± 0.25	0.88 ± 0.11	1.11 ± 0.27	1.34 ± 0.23	1.38 ± 0.23*	1.24 ± 0.23†
LVEDD, cm	4.50 ± 1.77	4.73 ± 0.54	4.52 ± 0.58	4.40 ± 0.59	4.28 ± 0.70	4.20 ± 0.55
LA area, cm^2	28.82 ± 6.20	15.10 ± 5.35	21.09 ± 4.59	27.06 ± 5.74	25.2 ± 5.63*	22.78 ± 4.54†
E-wave, cm/s	0.84 ± 0.20	0.79 ± 0.12	0.75 ± 0.16	0.85 ± 0.19	0.84 ± 0.25*	0.85 ± 0.21
A-wave, cm/s	0.50 ± 0.24	0.67 ± 0.17	0.73 ± 0.16	0.47 ± 0.23	0.46 ± 0.24*	0.55 ± 0.28†
E/A	2.92 ± 7.79	1.23 ± 0.25	1.05 ± 0.25	2.88 ± 5.52	4.12 ± 13.58	1.84 ± 1.07
Average E′, cm/s	0.10 ± 0.68	0.10 ± 0.05	0.09 ± 0.03	0.14 ± 0.06	0.25 ± 1.52	0.06 ± 0.02
E/E′	16 ± 8	13 ± 18	10 ± 4	16 ± 6	19 ± 9*	17 ± 8
E-wave deceleration time, ms	180 ± 56	181 ± 48	187 ± 45	183 ± 55	168 ± 62	184 ± 52
2-dimensional GLS	−11.6 ± 4.6	−18.8 ± 3.4	−17.7 ± 5.0	−11.4 ± 4.2	−8.8 ± 2.8*	−11.3 ± 4.6
CMR parameters						
LV mass, g	244 ± 77	114 ± 37	162 ± 76	252 ± 64	264 ± 89*	197 ± 65†
LV mass index, g/cm^2	130 ± 41	59 ± 12	84 ± 44	132 ± 33	149 ± 46*	103 ± 30†
Maximal IVS, mm	18 ± 5	8 ± 1	13 ± 4	20 ± 4	21 ± 4*	17 ± 4†
LVEDV, ml	131 ± 36	124 ± 25	132 ± 28	133 ± 36	128 ± 39	115 ± 26†
LVEDV index, ml/m^2	69 ± 18	66 ± 13	69 ± 13	70 ± 18	70 ± 22	61 ± 15†
LVESV, ml	60.65 ± 30.77	38.58 ± 12.24	43.47 ± 22.92	62.11 ± 30.41	65.75 ± 33.41*	44.66 ± 15.28†
LVESV index, ml/m^2	32 ± 16	20 ± 6	23 ± 13	32 ± 15	36 ± 18*	24 ± 9†
LVSV, ml	71 ± 20	85 ± 16	89 ± 23	71 ± 19	63 ± 16*	70 ± 20
LVSV index, ml/m^2	38 ± 10	45 ± 8	45 ± 11	37 ± 10	36 ± 8*	37 ± 12
LVEF, %	56 ± 14	69 ± 5	69 ± 11	55 ± 14	52 ± 14*	61 ± 11†
RV mass, g	77 ± 24	38 ± 12	48 ± 20	82 ± 21	80 ± 22*	63 ± 16†
RV mass index, g/m^2	41 ± 13	20 ± 6	26 ± 11	43 ± 11	44 ± 12*	33 ± 8†
RVEDV, ml	131 ± 36	124 ± 26	115 ± 22	135 ± 38	125 ± 34	114 ± 24†
RVEDV index, ml/m^2	70 ± 19	68 ± 13	62 ± 10	71 ± 20	69 ± 19	60 ± 12†
RVESV, ml	64 ± 30	45 ± 10	41 ± 15	68 ± 32	65 ± 27*	54 ± 19†
RVESV index, ml/m^2	34 ± 16	25 ± 5	22 ± 8	35 ± 17	36 ± 15*	28 ± 10†
RVSV, ml	67 ± 19	80 ± 18	74 ± 15	68 ± 19	58 ± 17*	61 ± 17†
RVSV index, ml/m^2	36 ± 10	43 ± 9	40 ± 8	36 ± 10	32 ± 9*	32 ± 9†
RVEF, %	53 ± 13	64 ± 3	65 ± 10	52 ± 13	49 ± 12*	54 ± 12
LA area, cm^2	31 ± 8	22 ± 4	25 ± 6	33 ± 9	29 ± 5*	26 ± 5†
RA area, cm^2	28 ± 8	20 ± 2	23 ± 5	30 ± 8	27 ± 6*	25 ± 6†
MAPSE, mm	8 ± 3	14 ± 2	11 ± 3	7 ± 2	6 ± 2*	7 ± 4
TAPSE, mm	13 ± 5	23 ± 3	22 ± 5	12 ± 4	11 ± 4*	14 ± 6†
ECV, %	59 ± 13	29 ± 3	39 ± 12	59 ± 10	66 ± 10*	53 ± 8†

Values are mean ± SD, %, or median (interquartile range). *$p < 0.05$ for trend (1-way analysis of variance) in patients with ATTR across different grades of uptake by Tc-DPD scintigraphy. †$p < 0.05$ AL vs. ATTR (Tc-DPD grade 2 and 3).

AL = light-chain amyloidosis; ATTR = transthyretin amyloidosis; CMR = cardiac magnetic resonance; ECV = extracellular volume; GLS = global longitudinal strain; IVS = interventricular septum; LA = left atrium; LPW = left posterior wall; LV = left ventricular; LVEDD = left ventricular end-diastolic diameter; LVEDV = left ventricular end-diastolic volume; LVEF = left ventricular ejection fraction; LVESV = left ventricular end systolic volume; LVSV = left ventricular stroke volume; MAPSE = mitral annular plane systolic excursion; NT-proBNP = N-terminal pro-B-type natriuretic peptide; RA = right atrium; RV = right ventricular; RVEDV = right ventricular end-diastolic volume; RVEF = right ventricular ejection fraction; RVESV = right ventricular end-systolic volume; RVSV = right ventricular stroke volume; TAPSE = tricuspid annular plane systolic excursion; Tc-DPD = ^{99m}Tc-3,3-diphosphono-1,2-propanodicarboxylic acid scintigraphy.

FIGURE 1 Morphology Patterns in Cardiac Transthyretin Amyloidosis

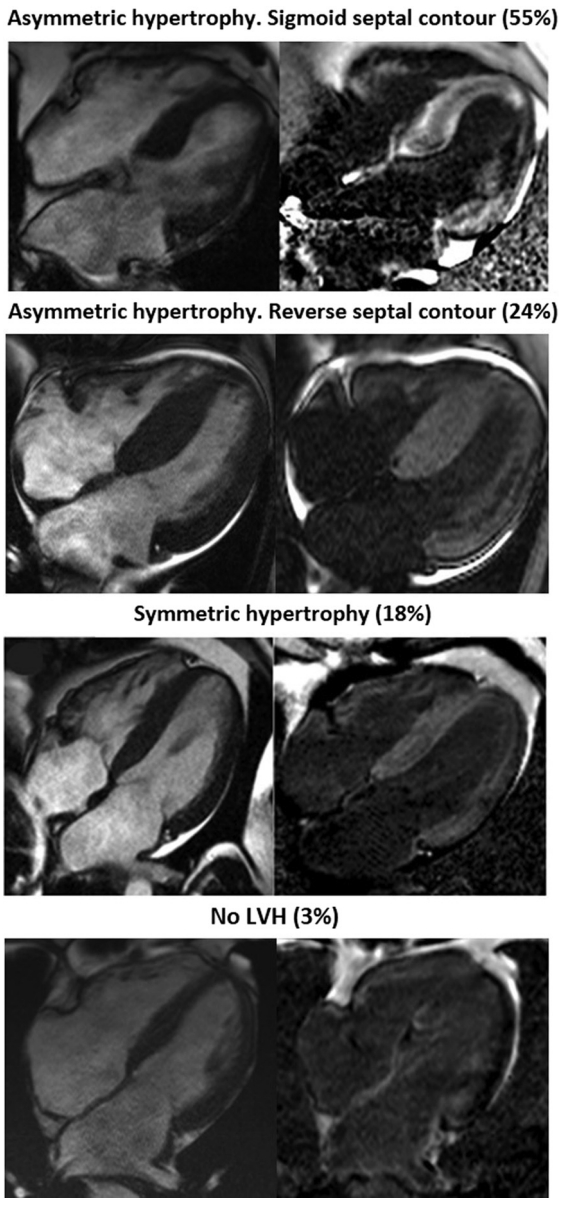

In 4 patients with cardiac transthyretin amyloidosis, 4-chamber cine image in diastole and corresponding late gadolinium enhancement (LGE) illustrate asymmetrical hypertrophy with sigmoid septal contour and transmural LGE; asymmetrical hypertrophy with reverse septal contour and transmural LGE; symmetrical hypertrophy pattern and transmural LGE; and no left ventricular hypertrophy (LVH) and subendocardial LGE.

RESULTS

The details of the 342 subjects are shown in Table 1. Of the 263 consecutive patients with ATTR, 168 had wild-type ATTR, and 95 had hereditary ATTR (ATTRm). Of the 17 patients with suspected cardiac ATTR, 9 had wild-type *TTR* gene sequence, and 8 had amyloidogenic *TTR* gene mutations. The *TTR* mutations in cardiac amyloidosis were as follows: V122I (n = 49); T60A (n = 26); V30M (n = 8); S77Y (n = 2); and E54G, E54L, E89K, D38Y, D39V, E89K, V20I, F44L, G89L, and L12P in 1 case each. The mutations among the possible cardiac amyloidosis subjects were as follows: S77Y (n = 3) and V30M, I107F, E54G, G47V, and I84S in 1 case each. Finally, the mutations among the mutation carriers were T60A (n = 6), V30M (n = 5), and S77Y (n = 1).

MORPHOLOGICAL PHENOTYPES. Asymmetrical septal hypertrophy, defined as a ratio between the septal and posterior wall >1.5 (19,28), was the most common form of ventricular remodeling in ATTR, being present in 79% of patients with cardiac ATTR. The pattern of asymmetrical septal hypertrophy was divided into the morphological subtypes of sigmoid septum (55%) and reverse septal contour (24%). Symmetrical concentric LVH, considered typical for amyloidosis, was present in only 18% of patients with ATTR (Figure 1). There were no differences in the prevalence of the different morphological phenotypes in wild-type ATTR and ATTRm (sigmoid septal 53% vs. 60%, reverse septal curvature 25% vs. 20%, and symmetrical concentric LVH 19% vs. 18%, respectively). Seven patients (3%) with cardiac ATTR amyloidosis (grade 2 or 3 cardiac uptake on ^{99m}Tc-DPD scintigraphy) had no LVH (2 with ATTRm and 5 with wild-type ATTR).

Prevalence of asymmetrical septal hypertrophy was significantly higher in ATTR than in patients with cardiac AL amyloidosis (79% vs. 14%; $p < 0.001$), for whom the most common form of ventricular remodeling was symmetrical concentric LVH (34 patients [68%]), followed by asymmetrical pattern with sigmoid septal contour in 7 patients (14%). The asymmetrical pattern with reverse septal contour was not found in the AL amyloidosis cohort. Nine patients (18%) with cardiac AL amyloidosis had no LVH.

TISSUE CHARACTERIZATION FINDINGS. In patients with cardiac amyloidosis, LGE was always present, and the pattern of LGE was typical for amyloidosis, being diffuse subendocardial LGE in 29% of patients and transmural LGE in 71% (Figure 2). Right ventricular (RV) LGE was extremely frequent, being present in 96% of patients. There was no difference in LGE prevalence between wild-type ATTR and ATTRm (transmural LGE 71% vs. 72% and subendocardial LGE 29% vs. 28%; $p > 0.05$ for both). As previously reported, the prevalence of transmural LGE and RV LGE was significantly higher in ATTR than in AL

FIGURE 2 LGE Patterns Correlating With T1 and ECV Measurements

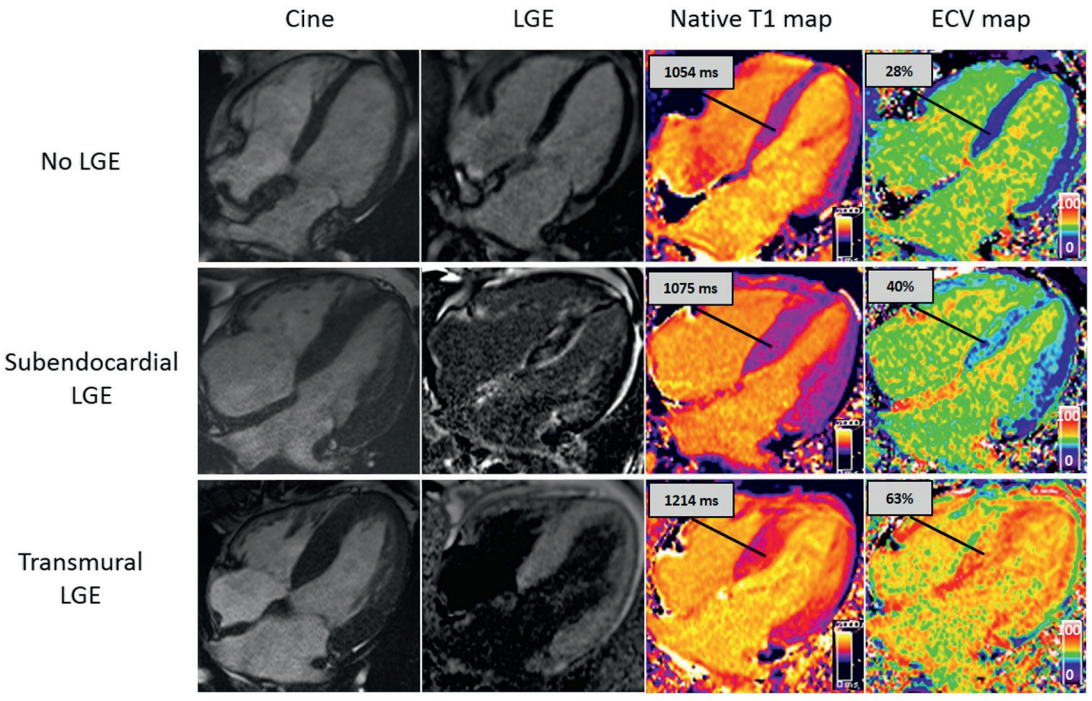

Images shown include 4-chamber cine, corresponding LGE image with phase-sensitive reconstruction, native T1 maps, and extracellular volume (ECV) maps in 3 patients with cardiac transthyretin amyloidosis. The patient with no LGE has normal native T1 and ECV maps; the patient with subendocardial LGE had borderline T1 values and high ECV values; and in the patient with transmural LGE, very high native T1 values and very high ECV values were seen. Abbreviations as in Figure 1.

(transmural LGE 71% vs. 50% and RV LGE 96% vs. 77%; $p < 0.01$ for both). In this population, transmural LGE was not associated with a worse prognosis than subendocardial LGE ($p = 0.327$).

Patients with suspected cardiac amyloidosis (17 patients with grade 1 uptake on ^{99m}Tc-DPD) did not show characteristic LGE of amyloidosis, with the notable exception of patients with the Se77Tyr variant (3 patients in our cohort with ^{99m}Tc-DPD grade 1). The rest of the patients showed no LGE ($n = 10$), subendocardial LGE with ischemic pattern ($n = 2$), and midwall LGE in the basal inferolateral wall ($n = 2$) (Online Figures 1 and 2). The 3 patients with Se77Tyr and ^{99m}Tc-DPD grade 1 had a typical LGE pattern (1 with subendocardial LGE and 2 with transmural LGE). The clinical, morphological, and functional features of these 3 patients were also in keeping with cardiac amyloidosis on echocardiogram, ECV measurements, and biomarkers (Figure 3), which suggests that they have less DPD uptake than they should given the amyloid burden.

There was good correlation between ECV and cardiac uptake on ^{99m}Tc-DPD scintigraphy ($r = 0.533$; $p < 0.05$). Except for patients with the Se77Tyr variant and grade 1 on ^{99m}Tc-DPD scintigraphy, ECV discriminated patients with ATTR with cardiac amyloidosis from patients with no or possible cardiac involvement (Figure 4). ECV was not significantly different in ATTRm compared with wild-type ATTR. When ECV was compared across the different mutations in patients with cardiac ATTR, patients with V30M had a significantly lower ECV than patients with wild-type ATTR, T60A, and V122I (42 ± 10% vs. 59 ± 11%, 54 ± 15%, and 64 ± 13%, respectively; all $p < 0.05$), and patients with V122I had significantly higher ECV than patients with V30M and T60A (65 ± 13% vs. 42 ± 10% and 54 ± 15%, respectively; all $p < 0.05$).

AMYLOID BURDEN AND SURVIVAL. At follow-up (19 ± 14 months), 65 of 292 subjects had died (36 with wild-type ATTR and 29 with ATTRm). ECV predicted death in the overall population (HR: 1.144; 95% CI: 1.075 to 1.218; $p < 0.001$) and separately in the wild-type ATTR and ATTRm groups ($p < 0.01$ for both) (Figure 5). ECV remained significantly associated with mortality (HR: 1.164; 95% CI: 1.066 to 1.271; $p < 0.01$) in

FIGURE 3 Patient With Cardiac Transthyretin Amyloidosis With Se77Tyr Variant

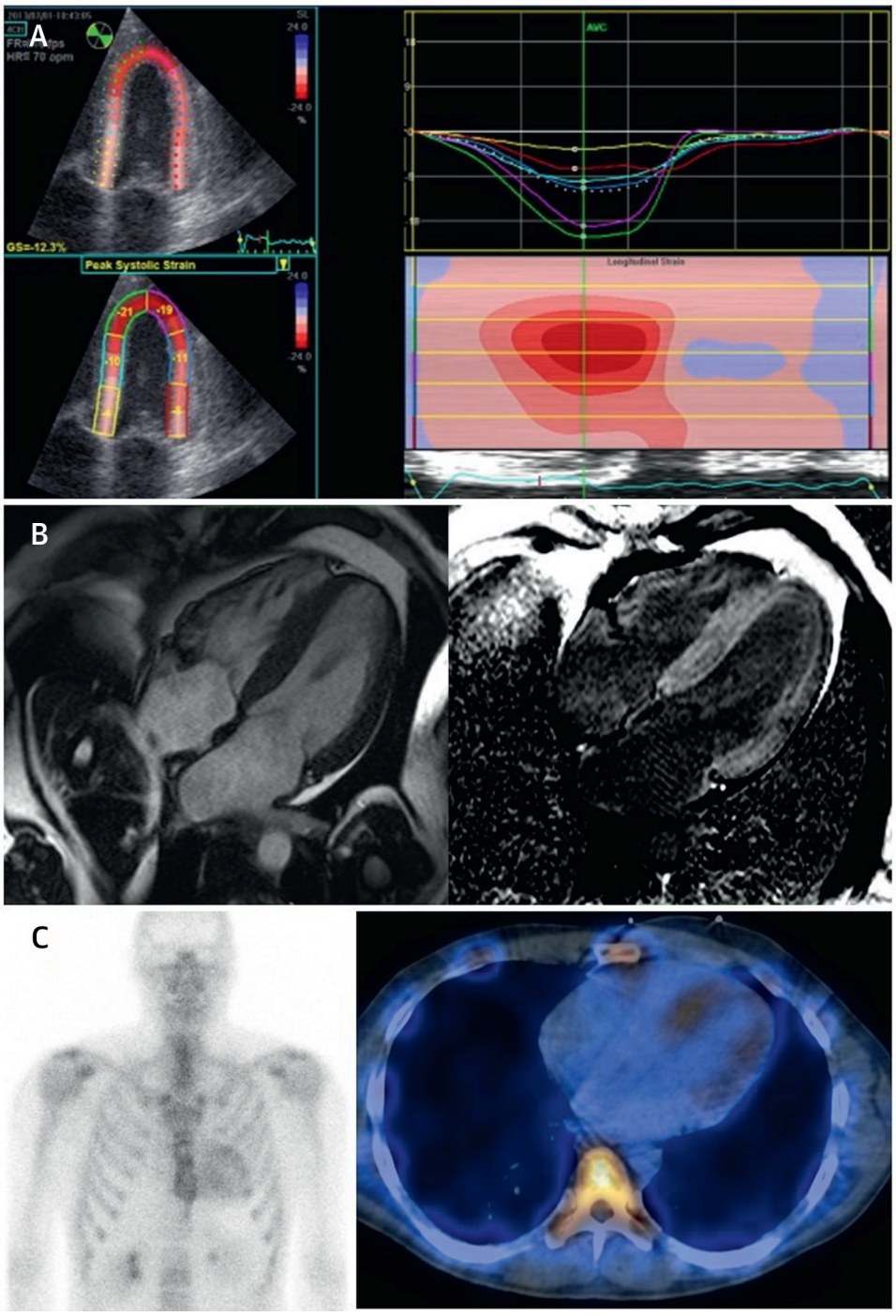

This multidisciplinary workup of a patient with cardiac transthyretin amyloidosis with an Se77Tyr variant displayed **(A)** a strain pattern characteristic of an infiltrative process; **(B)** a 4-chamber cine steady-state free precession image and corresponding LGE image showing transmural LGE; and **(C)** whole-body anterior ^{99m}Tc-3,3-diphosphono-1,2-propanodicarboxylic acid scintigraphy and hybrid single-photon emission computed tomography-computed tomography showing Perugini grade 1 abnormal uptake.

multivariable Cox models that included age, NT-proBNP, ejection fraction, E/E′, and LV mass index (troponin was not available in all patients) (Table 2).

DISCUSSION

In a prospective study at a single center, we describe here the specific morphological and tissue characteristics of ATTR cardiac amyloidosis using state-of-the-art imaging with CMR and identify what distinguishes it from AL and specific ATTR prognostic determinants.

This study had 3 major findings (Central Illustration). First, the morphological phenotype of patients with ATTR differed from AL and the one traditionally described, with asymmetrical LVH present in 79% of patients with ATTR amyloidosis versus 14% in AL amyloidosis. Reverse septal contour, classically associated with hypertrophic cardiomyopathy, was present in one-quarter of patients with ATTR. Additionally, LGE and ECV presented typical features in patients with ATTR, with very elevated ECV values and subendocardial or transmural LGE pattern. ECV correlated with cardiac uptake by ^{99m}Tc-DPD scintigraphy in all patients, except for those with the Se77Tyr mutation, for whom the degree of cardiac uptake on ^{99m}Tc-DPD scintigraphy stood out as being disproportionately low compared with the severity of cardiac involvement assessed by functional, structural, and clinical parameters. Finally, ECV predicted death and remained independently predictive after adjustment for known prognostic factors.

The LVH morphology in ATTR was surprising. The conventional view is that cardiac amyloidosis leads to symmetrically increased wall thickness. We suspect this happens for several reasons. The literature is heavily weighted toward AL, in which the morphology is mainly concentric, because ATTR until recently could only be diagnosed definitively by endomyocardial biopsy. Furthermore, patients with ATTR are typically elderly, and increased aortoseptal angulation could confound ascertainment, particularly by echocardiography. In addition, a focus on nomenclature, as to whether or not the wall thickening should be labeled as hypertrophy, might have prevented additional scrutiny. Looking further, we also note that the asymmetrical pattern with reverse septal contour was not found among the cardiac AL patients. This observation has important immediate diagnostic implications, because the association between amyloidosis and symmetrical septal hypertrophy could play an important role in the misdiagnosis of ATTR. One possibility that could explain why this pattern occurs is related to differential rates of effective cell hypertrophy in AL versus ATTR. Our prior work highlighted that in ATTR, total cell mass increased, whereas it remained the same in AL (29). It is possible that although infiltration was global, a triggered myocyte response differentially induced septal hypertrophy. Another possibility is that AL patients died before their total infiltration achieved the levels found in ATTR, so they were unable to get to the reverse septal contour stage.

We found that in all patients with cardiac ATTR, the pattern of LGE was always typical of cardiac amyloidosis, being subendocardial or transmural (25,30). Subendocardial LGE was found in 29%, and the remainder (71%) showed transmural LGE. RV LGE was present in 96% of patients. This confirmed previous reports on the high prevalence of transmural LGE and RV LGE in ATTR (31), but it also highlighted the important role that CMR could have in diagnosing this disease. The typical appearance of LGE in patients with cardiac ATTR with subendocardial or transmural LGE has the potential to revolutionize the diagnostic pathway of this disease, because CMR is currently the diagnostic reference standard for the differential diagnosis of cardiomyopathies with hypertrophic phenotype.

With the exception of patients with the Se77Tyr variant, none of the patients with suspected rather

FIGURE 4 ECV and Cardiac Uptake

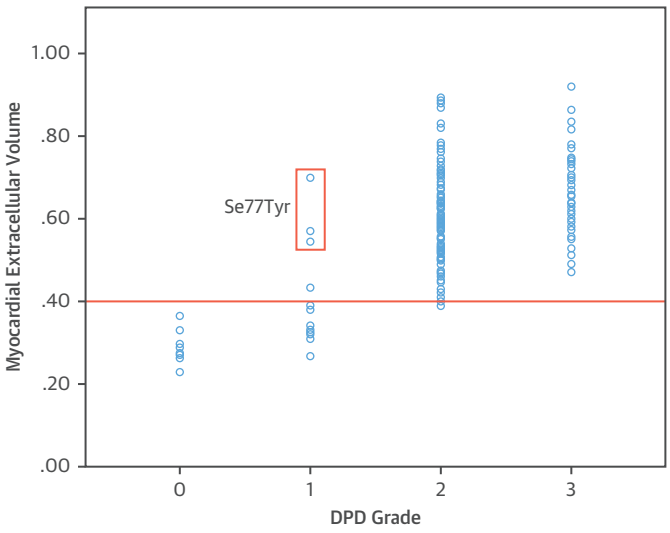

As seen in this correlation between ECV and grade of abnormal cardiac uptake on ^{99m}Tc-3,3-diphosphono-1,2-propanodicarboxylic acid scintigraphy, only patients with the Se77Tyr variant had high ECV measurements with grade 1 abnormal uptake. DPD = 3,3-diphosphono-1,2-propanodicarboxylic acid; ECV = extracellular volume.

FIGURE 5 Survival Analysis

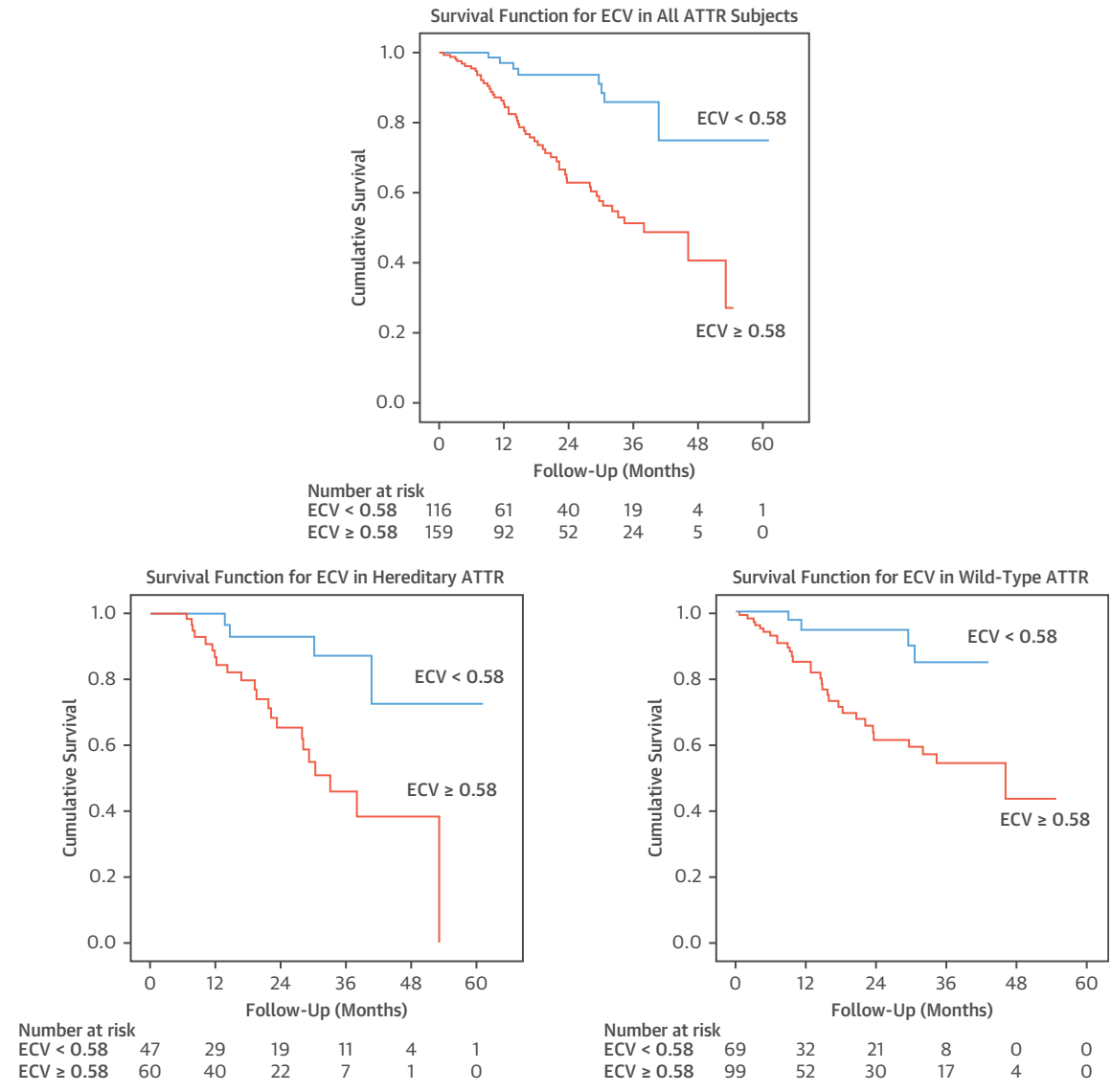

As seen via Kaplan-Meier curves, extracellular volume (ECV) was independently correlated with mortality in all patients with cardiac transthyretin amyloidosis (ATTR), as well as those with hereditary and wild-type ATTR.

than proven cardiac ATTR (defined as grade 1 cardiac uptake on ^{99m}Tc-DPD scintigraphy) showed LVH, typical LGE, or very elevated ECV (although a mild elevation in ECV was noted). In patients with the Se77Tyr variant and grade 1 cardiac uptake on ^{99m}Tc-DPD scintigraphy, CMR showed typical features of cardiac involvement, with LVH, characteristic LGE, and increased ECV. As assessed by functional, structural, and clinical parameters, there was good agreement between the CMR characterization of the degree of cardiac involvement and the echocardiographic

TABLE 2 Multivariable Analysis of Mortality Risk in Patients With ATTR

	HR (95% CI)	p Value
Age	1.059 (1.016-1.013)	<0.01
LV mass, each 10 g increase	0.941 (0.853-1.039)	0.229
LVEF, each 3% increase	0.986 (0.916-1.060)	0.699
NT-proBNP, each 100 pmol/l increase	1.016 (1.005-1.027)	<0.01
E/E′, each 1-U increase	0.996 (0.949-1.045)	0.873
ECV, each 3% increase	1.164 (1.066-1.271)	<0.01

CI = confidence interval; HR = hazard ratio; other abbreviations as in Table 1.

CENTRAL ILLUSTRATION **CMR in ATTR**

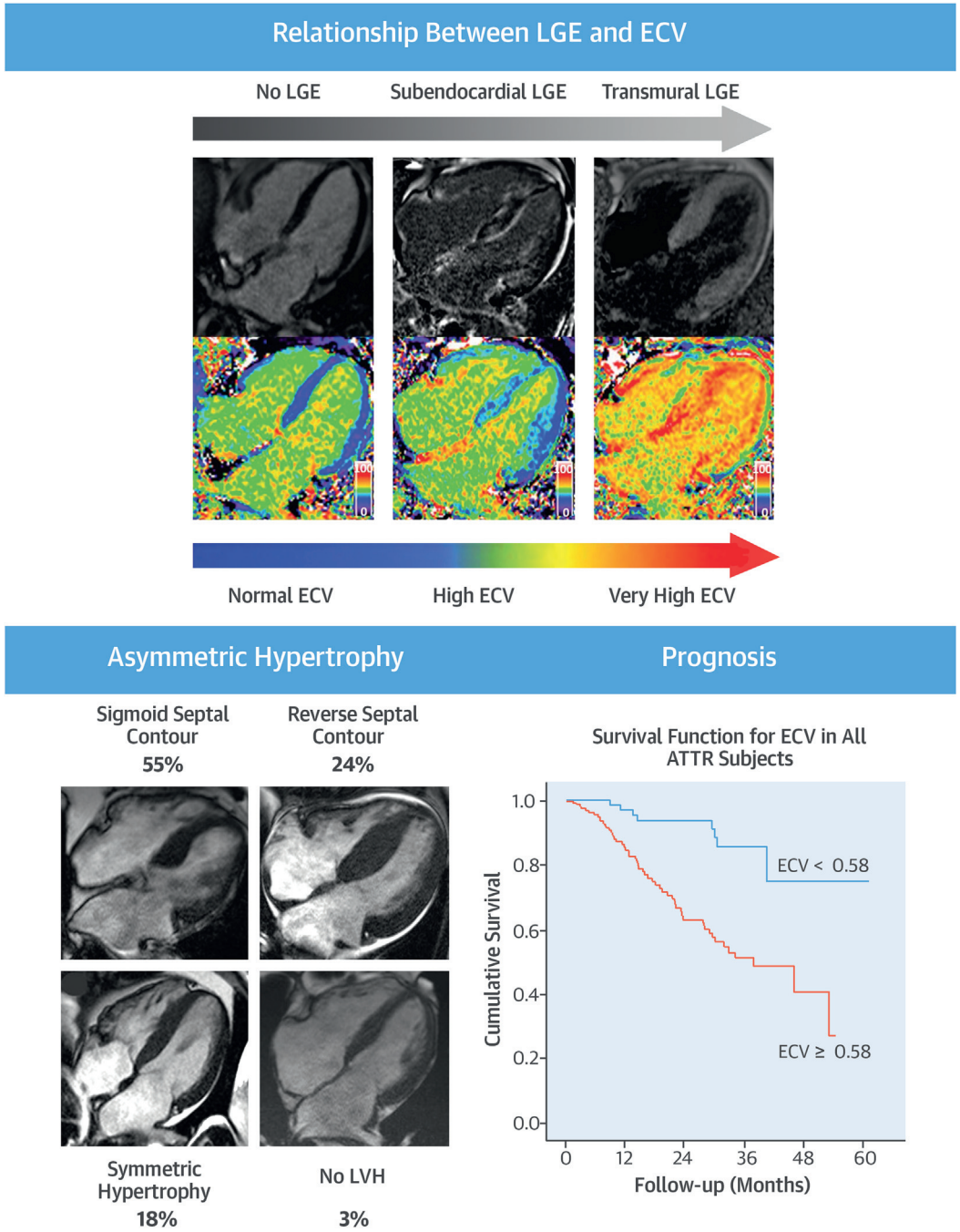

Martinez-Naharro, A. et al. J Am Coll Cardiol. 2017;70(4):466–77.

In this study, cardiac magnetic resonance (CMR) with extracellular volume (ECV) was used to characterize cardiac involvement as it related to outcomes in cardiac transthyretin amyloidosis (ATTR). The relationship between late gadolinium enhancement (LGE) patterns and ECV showed a typical correlation of very high ECV values and subendocardial or transmural LGE. Asymmetrical septal left ventricular hypertrophy (LVH) was present in 79% of patients with ATTR, >5 times more frequently than in patients with cardiac light-chain amyloidosis. In patients with ATTR, ECV was independently correlated with mortality.

and clinical features, although a discrepancy was observed with the degree of cardiac uptake on ^{99m}Tc-DPD scintigraphy that had been disproportionately low (**Figure 3**). The mechanism for this phenomenon remains unknown, but it raises the possibility of the degree of cardiac uptake being variant dependent.

ECV is the first noninvasive method for quantifying the cardiac interstitium, and several papers have shown correlation with markers of disease severity in both types of cardiac amyloidosis (16,32,33). When ECV was compared across the different mutations in patients with cardiac ATTR, patients with V30M had a significantly lower ECV than patients with wild-type ATTR, T60A, and V122I. The disease associated with the TTR V30M variant usually causes a predominant sensorimotor peripheral neuropathy and autonomic neuropathy. Although cardiac amyloidosis might occur in older patients with this TTR variant, the vast majority of patients have minor degrees of cardiac involvement or, in younger affected individuals, none at all. Therefore, the lower ECV likely represents the different clinical phenotype of this variant compared with other variants that are characterized by predominantly cardiac features (even though the neurological phenotype can coexist). The prognostic value of ECV in AL amyloidosis was recently shown (33), and here, for the first time, we have demonstrated that ECV adds incremental value over and above existing clinical markers in ATTR. ECV was predictive regardless of whether patients were presenting at diagnosis or years into the disease process, which highlights the potential use of the ECV to assess disease status throughout the course of disease progression. A spectrum of disease burden exists, ranging from small incidental deposits with no clinical consequence to very extensive deposits causing severe organ failure. LGE can confirm the diagnosis and divide patients with cardiac amyloidosis into groups that likely represent different stages of myocardial infiltration, with the transmural pattern being associated with a higher ECV than the subendocardial one. ECV can measure the continuum of amyloid infiltration, enabling the clinician to fully characterize phenotypes, their stages of evolution, and the prognostic implication of amyloid deposition (**Figure 2**). The better prognostic ability of ECV compared with LGE likely springs from the better discriminatory powers of ECV, which can measure the continuum of infiltration rather than a binary categorization. Some patients in the cohort had a modest ECV increase without evidence of cardiac involvement by echocardiogram, LGE, or blood biomarkers; this suggests that as in AL, ECV can detect early cardiac involvement (29). The presence of low-grade disease was also confirmed by a low degree of cardiac uptake on the ^{99m}Tc-DPD scintigraphy that seemed to show a similar sensitivity.

STUDY LIMITATIONS. We used the proposed noninvasive criteria for ATTR (9), which means a cardiac biopsy was performed only in a minority of patients. Two different T1 mapping techniques were used during the period in which these patients were recruited, and a wide range of *TTR* mutations were included in the analysis.

CONCLUSIONS

The morphological phenotype of patients with ATTR was different from the one traditionally described: asymmetrical LVH was the commonest pattern of ventricular hypertrophy in cardiac ATTR, with reverse septal contour, classically associated with hypertrophic cardiomyopathy, being present in one-quarter of patients with ATTR. LGE and ECV presented typical features in patients with ATTR amyloidosis, with very elevated ECV values and subendocardial or transmural LGE pattern. ECV, a noninvasive quantification of the cardiac amyloid burden, predicted death and remained an independent predictor of prognosis after adjustment for known prognostic factors.

ACKNOWLEDGMENTS The authors are thankful for the contributions of patients, the administrative and nursing staff, histopathologists, geneticists, echocardiographers, nuclear medicine technologists, and radiographers at the National Amyloidosis Centre and Heart Centre.

ADDRESS FOR CORRESPONDENCE: Dr. Marianna Fontana, National Amyloidosis Centre, University College London, Royal Free Hospital, Rowland Hill Street, London NW3 2PF, United Kingdom. E-mail: m.fontana@ucl.ac.uk.

PERSPECTIVES

COMPETENCY IN MEDICAL KNOWLEDGE: The morphological phenotype of patients with ATTR is most commonly characterized by asymmetrical LVH. LGE and high ECV fraction are typical features on CMR. Measurement of ECV by this method is a noninvasive index of cardiac amyloid burden and an independent predictor of prognosis.

TRANSLATIONAL OUTLOOK: Future characterization of patients with ATTR by CMR could identify earlier features of the disease, which is an underrecognized cause of heart failure in the elderly.

REFERENCES

1. Rapezzi C, Quarta CC, Riva L, et al. Transthyretin-related amyloidoses and the heart: a clinical overview. Nat Rev Cardiol 2010;7:398–408.

2. Cornwell GG 3rd, Murdoch WL, Kyle RA, Westermark P, Pitkänen P. Frequency and distribution of senile cardiovascular amyloid: a clinicopathologic correlation. Am J Med 1983;75:618–23.

3. Ruberg FL, Berk JL. Transthyretin (TTR) cardiac amyloidosis. Circulation 2012;126:1286–300.

4. Jacobson DR, Pastore RD, Yaghoubian R, et al. Variant-sequence transthyretin (isoleucine 122) in late-onset cardiac amyloidosis in black Americans. N Engl J Med 1997;336:466–73.

5. Pinney JH, Whelan CJ, Petrie A, et al. Senile systemic amyloidosis: clinical features at presentation and outcome. J Am Heart Assoc 2013;2:e000098.

6. Pinney JH, Smith CJ, Taube JB, et al. Systemic amyloidosis in England: an epidemiological study. Br J Haematol 2013;161:525–32.

7. Bokhari S, Castaño A, Pozniakoff T, Deslisle S, Latif F, Maurer MS. ^{99m}Tc-pyrophosphate scintigraphy for differentiating light-chain cardiac amyloidosis from the transthyretin-related familial and senile cardiac amyloidoses. Circ Cardiovasc Imaging 2013;6:195–201.

8. Castaño A, DeLuca A, Weinberg R, et al. Serial scanning with technetium pyrophosphate (99mTc-PYP) in advanced ATTR cardiac amyloidosis. J Nucl Cardiol 2016;23:1355–63.

9. Gillmore JD, Maurer MS, Falk RH, et al. Nonbiopsy diagnosis of cardiac transthyretin amyloidosis. Circulation 2016;133:2404–12.

10. Hutt DF, Fontana M, Burniston M, et al. Prognostic utility of the Perugini grading of 99mTc-DPD scintigraphy in transthyretin (ATTR) amyloidosis and its relationship with skeletal muscle and soft tissue amyloid. Eur Heart J Cardiovasc Imaging 2017 Feb 4 [E-pub ahead of print].

11. Wechalekar AD, Gillmore JD, Hawkins PN. Systemic amyloidosis. Lancet 2016;387:2641–54.

12. Banypersad SM, Sado DM, Flett AS, et al. Quantification of myocardial extracellular volume fraction in systemic AL amyloidosis: an equilibrium contrast cardiovascular magnetic resonance study. Circ Cardiovasc Imaging 2013;6:34–9.

13. Karamitsos TD, Piechnik SK, Banypersad SM, et al. Noncontrast T1 mapping for the diagnosis of cardiac amyloidosis. J Am Coll Cardiol Img 2013;6:488–97.

14. Fontana M, Banypersad SM, Treibel TA, et al. Native T1 mapping in transthyretin amyloidosis. J Am Coll Cardiol Img 2014;7:157–65.

15. Schelbert EB, Messroghli DR. State of the art: clinical applications of cardiac T1 mapping. Radiology 2016;278:658–76.

16. Barison A, Aquaro GD, Pugliese NR, et al. Measurement of myocardial amyloid deposition in systemic amyloidosis: insights from cardiovascular magnetic resonance imaging. J Intern Med 2015;277:605–14.

17. Robbers LF, Baars EN, Brouwer WP, et al. T1 mapping shows increased extracellular matrix size in the myocardium due to amyloid depositions. Circ Cardiovasc Imaging 2012;5:423–6.

18. Brooks J, Kramer CM, Salerno M. Markedly increased volume of distribution of gadolinium in cardiac amyloidosis demonstrated by T1 mapping. J Magn Reson Imaging 2013;38:1591–5.

19. Pozo E, Kanwar A, Deochand R, et al. Cardiac magnetic resonance evaluation of left ventricular remodelling distribution in cardiac amyloidosis. Heart 2014;100:1688–95.

20. Gillmore JD, Wechalekar A, Bird J, et al. Guidelines on the diagnosis and investigation of AL amyloidosis. Br J Haematol 2015;168:207–18.

21. Fontana M, White SK, Banypersad SM, et al. Comparison of T1 mapping techniques for ECV quantification: histological validation and reproducibility of ShMOLLI versus multibreath-hold T1 quantification equilibrium contrast CMR. J Cardiovasc Magn Reson 2012;14:88.

22. White SK, Sado DM, Fontana M, et al. T1 mapping for myocardial extracellular volume measurement by CMR: bolus only versus primed infusion technique. J Am Coll Cardiol Img 2013;6:955–62.

23. Lever HM, Karam RF, Currie PJ, Healy BP. Hypertrophic cardiomyopathy in the elderly. Distinctions from the young based on cardiac shape. Circulation 1989;79:580–9.

24. Solomon SD, Wolff S, Watkins H, et al. Left ventricular hypertrophy and morphology in familial hypertrophic cardiomyopathy associated with mutations of the beta-myosin heavy chain gene. J Am Coll Cardiol 1993;22:498–505.

25. Fontana M, Pica S, Reant P, et al. Prognostic value of late gadolinium enhancement cardiovascular magnetic resonance in cardiac amyloidosis. Circulation 2015;132:1570–9.

26. Hutt DF, Quigley AM, Page J, et al. Utility and limitations of 3,3-diphosphono-1,2-propanodicarboxylic acid scintigraphy in systemic amyloidosis. Eur Heart J Cardiovasc Imaging 2014;15:1289–98.

27. Perugini E, Guidalotti PL, Salvi F, et al. Noninvasive etiologic diagnosis of cardiac amyloidosis using ^{99m}Tc-3,3-diphosphono-1,2-propanodicarboxylic acid scintigraphy. J Am Coll Cardiol 2005;46:1076–84.

28. Florian A, Masci PG, De Buck S, et al. Geometric assessment of asymmetric septal hypertrophic cardiomyopathy by CMR [published correction appears in J Am Coll Cardiol Img 2012;5:968]. J Am Coll Cardiol Img 2012;5:702–11.

29. Fontana M, Banypersad SM, Treibel TA, et al. Differential myocyte responses in patients with cardiac transthyretin amyloidosis and light-chain amyloidosis: a cardiac MR imaging study. Radiology 2015;277:388–97.

30. Maceira AM, Joshi J, Prasad SK, et al. Cardiovascular magnetic resonance in cardiac amyloidosis. Circulation 2005;111:186–93.

31. Dungu JN, Valencia O, Pinney JH, et al. CMR-based differentiation of AL and ATTR cardiac amyloidosis. J Am Coll Cardiol Img 2014;7:133–42.

32. Bandula S, Banypersad SM, Sado D, et al. Measurement of tissue interstitial volume in healthy patients and those with amyloidosis with equilibrium contrast-enhanced MR imaging. Radiology 2013;268:858–64.

33. Banypersad SM, Fontana M, Maestrini V, et al. T1 mapping and survival in systemic light-chain amyloidosis. Eur Heart J 2015;36:244–51.

KEY WORDS ATTR, extracellular volume fraction, late gadolinium enhancement, left ventricular hypertrophy, N-terminal pro-B-type natriuretic peptide

APPENDIX For supplemental figures, please see the online version of this article.